Zinc-blende–wurtzite polytypism in semiconductors

Chin-Yu Yeh, Z. W. Lu, S. Froyen, and Alex Zunger
National Renewable Energy Laboratory, Golden, Colorado 80401
(Received 16 July 1992)

The zinc-blende (ZB) and wurtzite (W) structures are the most common crystal forms of binary octet semiconductors. In this work we have developed a simple scaling that systematizes the $T=0$ energy difference ΔE_{W-ZB} between W and ZB for all simple binary semiconductors. We have first calculated the energy difference $\Delta E^{LDF}_{W-ZB}(AB)$ for AlN, GaN, InN, AlP, AlAs, GaP, GaAs, ZnS, ZnSe, ZnTe, CdS, C, and Si using a numerically precise implementation of the first-principles local-density formalism (LDF), including structural relaxations. We then find a *linear* scaling between $\Delta E^{LDF}_{W-ZB}(AB)$ and an atomistic orbital-radii coordinate $\bar{R}(A,B)$ that depends only on the properties of the free atoms A and B making up the binary compound AB. Unlike classical structural coordinates (electronegativity, atomic sizes, electron count), $\bar{R}$ is an orbital-dependent quantity; it is calculated from atomic pseudopotentials. The good linear fit found between ΔE_{W-ZB} and $\bar{R}$ (rms error of ~ 3 meV/atom) permits predictions of the W−ZB energy difference for many more AB compounds than the 13 used in establishing this fit. We use this model to identify chemical trends in ΔE_{W-ZB} in the IV-IV, III-V, II-VI, and I-VII octet compounds as either the anion or the cation are varied. We further find that the ground state of MgTe is the NiAs structure and that CdSe and HgSe are stable in the ZB form. These compounds were previously thought to be stable in the W structures.

I. INTRODUCTION

Zinc blende (ZB) and wurtzite (W) are the most common crystal structures of binary octet semiconductors.[1–5] Figure 1 depicts three views of the structural differences between these forms: they differ in the relative handedness of the fourth interatomic bond along the (111) chain ["right" and "left" for W and ZB, respectively, see Figs. 1(a) and 1(b)] or, equivalently, in their dihedral conformation ["eclipsed" and "staggered" for W and ZB, respectively, see Figs. 1(c) and 1(d)]. Figures 1(e) and 1(f) shows the layer stacking along (111), exhibiting an $ABABABA\ldots$ sequence for W and an $ABCABCA\ldots$ sequence for ZB. These rather subtle structural differences and the attendant small difference in the internal energies ($\lesssim 20$ meV/atom) are manifested by the well-known W−ZB polytypism:[2–5] depending on the details of the growth parameters, a number of binary semiconductors (SiC, CdS, CdSe, ZnS, CuCl, and CuBr) can be prepared at ambient pressure in either forms.[4b] Despite these structural similarities between W and ZB, their spectroscopic characteristics can be very different: for example, the minimum low-temperature band gaps of SiC in the W and ZB forms are 3.33 (Ref. 6) and 2.42 eV,[7] respectively, and their phonon frequencies show large systematic variations.[6] Consequently, recent interest in optical application of wide-gap III-V and II-VI semiconductors[8] has raised the need to systematize the W vs ZB structural preferences among binary semiconductors. In this paper we investigate the intrinsic W vs ZB energy differences and the systematics in this quantity among binary octet compounds.

An experimental assessment of the W vs ZB order of stability at low temperature is possible when *bulk* phase diagram data are available. For example, the bulk phase diagrams of Cu monohalides,[9] of CdSe,[10] and ZnS (Ref. 11) clearly demonstrate that ZB is the stable low-temperature phase and that this phase transforms reversi-

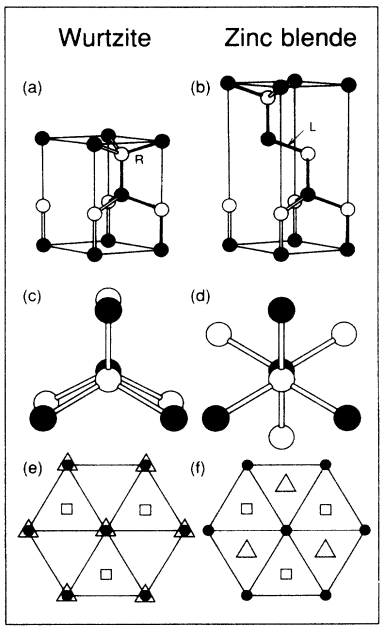

FIG. 1. Three views of the difference between the wurtzite and zinc-blende crystal structures. (a) and (b) show the handedness of the fourth interatomic bond along the right (R) for W and left (L) for ZB. (c) and (d) show the "eclipsed" and "staggered" dihedral conformations for W and ZB. (e) and (f) show the layer stacking along (111).

bly into the W structure above a critical temperature T_c. For ZnS, CdSe, CuCl, CuBr, and CuI, $T_c = 1020 \pm 5\,^{\circ}\mathrm{C}$,[11] $95 \pm 5\,^{\circ}\mathrm{C}$,[10] and 407, 386, and 396 °C, respectively.[9] The determination of the intrinsically stabler crystal modification is difficult, however, when (i) neither W nor ZB is the stable low-temperature phase (e.g., in MgO, MgS, MgSe, MnO, and CdO the low-temperatures ground state is the NaCl structure), or when (ii) only *epitaxial* growth parameters are known. We are nevertheless interested in examining the intrinsic W vs Zb structural stability in as many cases as possible (even if neither is the ground state).

Epitaxially induced distortions of the bulk stability are manifested in two ways. First, even if the equilibrium molar volumes of the bulk W and ZB modifications of a given compound are similar, on a (001) ZB substrate it is geometrically possible to grow only the ZB form as a defect-free film; the W form growing on such a substrate will necessarily have fivefold- and sixfold-coordinated atoms whose large defect formation energies will suppress growth of the W form. Hence, growth of CdSe,[12] ZnTe,[13] ZnSe, and ZnS (Ref. 14) on a (001) GaAs substrate results invariably in the ZB form irrespective of the intrinsic W-ZB energy difference. In such cases, the atomic topology of the (001)-oriented substrate "templet" overrules the intrinsic W vs ZB bulk stability, selecting the topologically compatible ZB form. Such a selectivity does not exist on a (111)-oriented ZB substrate, where growth of either W or ZB is geometrically possible without producing miscoordinated atoms. On such substrates we encounter the second epitaxial deformation effect, namely "epitaxial size selectivity":[15] the variant that grows is the one having the best elastic match with the substrate, often in defiance of the relative *bulk* stabilities. This mechanism was discussed by Froyen, Wei, and Zunger,[15] who proposed epitaxial conditions that will stabilize the β-Sn structure of CdTe, and the ZB structure of MgS and NaCl (the stable bulk structures are ZB, NaCl, and NaCl, respectively). Experimental manifestations of such "epitaxial size selectivity" effects include the growth of the NaCl form of cesium and thallium halides on mica and other substrates,[16] the W form of MgS and MgSe evaporated on alkali halides and metal substrates,[17,18] the NaCl form of InSb obtained by sputtering,[19] and the ZB form of GaN grown on MgO.[20]

Taking such considerations into account, it is possible to assess from phase diagram and crystal growth data the most stable bulk crystal structure at low temperature for many octet compounds. This is summarized in Fig. 2. We wish to study *quantitatively* the W vs ZB energy differences in these compounds (whether these are the stablest crystal forms or not) and identify the major chemical trends as either the anion or the cation are changed.

A *qualitative* systematization of structural trends such as those seen in Fig. 2 has largely been accomplished following the introduction of the nonclassical structural coordinate scales of Phillips[21] (the homopolar and heteropolar dielectric band gaps E_h and C) and the orbital radii of St. John and Bloch,[22] Zunger and Cohen,[23,24] and Chelikowsky and Phillips.[25] The orbital radii coordinates

	O	S	Se	Te
Be	W	ZB	ZB	ZB
Mg	NaCl	NaCl	NaCl	W
Ca	NaCl	NaCl	NaCl	NaCl
Mn	NaCl	NaCl	NaCl	NiAs
Zn	W	ZB	ZB	ZB
Cd	NaCl	W	ZB	ZB
Hg	Cinb	Cinb	ZB	ZB

	N	P	As	Sb
B	Graphite	ZB	ZB	*****
Al	W	ZB	ZB	ZB
Ga	W	ZB	ZB	ZB
In	W	ZB	ZB	ZB

FIG. 2. The experimentally stable crystal structure of octet AB compounds, W=wurtzite, ZB=zinc blende, Cinb.=cinnabar, ***** means that the compound does not exist. a_0 means the Bohr radius.

are linear combinations

$$R_\sigma(A,B) = |(r_p^A + r_s^A) - (r_p^B + r_s^B)| ,$$
$$R_\pi(A,B) = |r_p^A - r_s^A| + |r_p^B - r_s^B| , \tag{1}$$

of the classical crossing points $r_l^{A,B}$ of the screened nonlocal atomic pseudopotentials of angular momentum l. It was previously demonstrated[22–25] that in the $R_\sigma(A,B)$ vs $R_\pi(A,B)$ plane there exists a separation into simple regions occupied predominantly by compounds belonging to a single structure. The orbital radii determined from *ab initio* local-density formalism[23,24] were first applied to 565 binary (octet and nonoctet) 1:1 AB compounds, achieving a $>95\%$ successful separation of 35 structure types. Later, these radii were incorporated into the 3-coordinate scale of Villars and co-workers[26] and used to systematize the crystal structures of nearly 6000 binary, ternary, and quaternary intermetallic compounds and binary oxides and halides. Recent work includes applications of these *ab initio* radii to quasicrystals and high-T_c superconductors.[27]

Figure 3 illustrates the structural separation maps for the binary octet compounds considered here using (a) Eq. (1) with the local-density pseudopotential orbital radii $\{r_l\}$ of Zunger and Cohen,[23,24] (b) Eq. (1) with the radii at which the all-electron atomic radial orbitals $rR_{nl}(r)$ have their outer maxima, and (c) a dual coordinate map using Phillips' dielectric electronegativity variables $C(AB)$ and $E_h(AB)$ (the latter map has been redrawn since in the original reference[21] CuCl, CuBr, AgI, and CdSe have been incorrectly labeled as being stable in the W form). The 3-coordinate diagram of Villars[26] is not shown since it produces no improvement over Fig. 3(a) for the octet ZB-W system. We see that in all three cases shown in Fig. 3 one can draw simple straight-line boundaries that

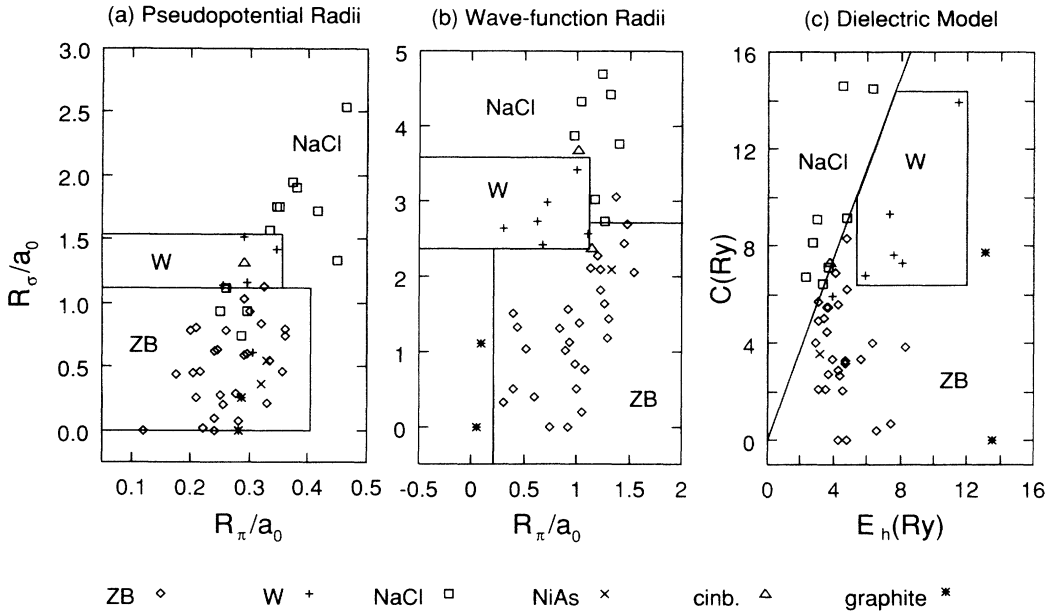

FIG. 3. Structural separation maps for binary octet compounds from (a) pseudopotential orbital radii (Refs. 23 and 24), (b) wave-function orbital radii, and (c) Phillips dielectric model (Ref. 21). (b) and (c) do not include the MnX (X: O, S, Se, and Te) compounds, and (c) does not include HgO.

delineate compounds stable in a given crystal structure. There are a number of "misplaced" compounds in these diagrams. For example, the pseudopotential orbital radii plot [Fig. 3(a)] incorrectly places BeO and MnS+MnSe+MgS+MgSe in the ZB region instead of in the W and NaCl domains, respectively. The wave-function maximum radii plot [Fig. 3(b)] places CuCl in the NaCl domain (instead of in the ZB domain), and Phillips' scale places CdS in the ZB (rather than in the W) domain. Overall, however, it is remarkable that *elemental* coordinates are able to produce such a delicate structure separation.

As successful as these diagrammatic structural maps are, they provide but a binary (yes/no) answer to the question "is X the stable crystal structure of a given compound?" In the absence of a systematic database of *structural energy differences* $\Delta E_{\alpha\beta}(AB)=E_\alpha(AB)-E_\beta(AB)$ for a series of compounds $\{AB\}$ in different crystal structures α and β, it was impossible to establish whether a scaling exists between the structural coordinates shown in Fig. 3 and $\Delta E_{\alpha\beta}(AB)$. Indeed, *quantitative* structural regularities within homological chemical sequences (whose members have the same structure) such as AlN→GaN→InN or AlN→AlP→AlAs→AlSb cannot be established unless such a scaling is known. Furthermore, if neither α nor β are the stable crystal structure of AB, structural diagrams provide no hint on the energy difference $\Delta E_{\alpha\beta}(AB)$ or the relative order of such unstable (or metastable) phases.

In order to address such questions we have calculated the $T=0$, W−ZB energy difference

$$\Delta E^{\rm LDF}_{\rm W-ZB}(AB)=E^{\rm LDF}_{\rm W}(AB)-E^{\rm LDF}_{\rm ZB}(AB) \quad (2)$$

for 13 AB compounds belonging to the IV-IV, III-V, and II-VI groups, using a numerically precise implementation[28,29] of the local-density formalism (LDF). We discovered a simple *linear* scaling between an "effective orbital ionicity"

$$\tilde{R}(A,B)=\tilde{R}_\sigma(A,B)+\lambda\tilde{R}_\pi(A,B) \quad (3)$$

and the model (M) W−ZB energy difference, i.e.,

$$\Delta E^{\rm LDF}_{\rm W-ZB}(AB)\cong\Delta E^{M}_{\rm W-ZB}(AB)\equiv E_0+\alpha\tilde{R}(A,B)\ , \quad (4)$$

where $\tilde{R}_\sigma$ and $\tilde{R}_\pi$ for atomistic coordinates related to the orbital radii [Eq (1)]. Like in Eq. (1), the determination of $\tilde{R}_\sigma(A,B)$ and $\tilde{R}_\pi(A,B)$ requires only the knowledge of *free atom* (A and B) quantities; these can be calculated once and for all either from atomic wave functions or from nonlocal atomic pseudopotentials.[24] The model of Eq. (4) then permits quantitative predictions of the W−ZB energy differences for many more binary octet compounds than we directly calculated (including cases for which neither W nor ZB are the ground states) and unravels simple chemical trends as a function of the position of A and B in the Periodic Table. This is then used to articulate new "chemical rules" pertaining to the W vs ZB stability among all binary octet compounds. A preliminary account of this work was recently published.[30]

II. CALCULATING THE W−ZB TOTAL-ENERGY DIFFERENCES

We calculated $\Delta E^{\rm LDF}_{\rm W-ZB}$ of Eq. (2) for 13 compounds. These include compounds that are known to be highly stable in the W structure[4,5] (AlN, GaN, and InN) and compounds that occur at low temperatures only in the zinc-blende (or diamond) phase[1-5] (Si, AlP, AlAs, GaP, GaAs, and ZnTe). We then add compounds known to exhibit W−ZB polytypism (ZnS, ZnSe, and CdS), and

carbon, whose ground state (graphite) is neither W nor ZB.

The W−ZB total-energy difference of Eq. (2) was calculated in the LDF using the Ceperley-Alder[31(a)] exchange correlation as parametrized by Perdew and Zunger.[31(b)] We used the plane-wave nonlocal pseudopotential method[28] for Si and the III-V's and the linearized-augmented-plane-wave (LAPW) method[29] for C and the II-VI's (whose core d states are difficult to converge in a pure plane-wave basis). We use Kerber's method [Ref. 31(c)] to calculate the pseudopotential and apply the nonlinear core correction [Ref. 31(d)].

The lattice parameters of the ZB and W crystal structures are optimized to reach a minimum in the total energies. The unit-cell vectors for the ZB structure are

$$\begin{aligned} \mathbf{a}&=(0,\tfrac{1}{2},\tfrac{1}{2})a\ , \\ \mathbf{b}&=(\tfrac{1}{2},0,\tfrac{1}{2})a\ , \\ \mathbf{c}&=(\tfrac{1}{2},\tfrac{1}{2},0)a\ , \end{aligned} \tag{5}$$

where a is the cubic lattice constant. There are two atoms per unit cell: A at $(0,0,0)a$ and B at $(\frac{1}{4},\frac{1}{4},\frac{1}{4})a$. Hence, only the value of a needs to be optimized. For the W structure, the lattice vectors are

$$\begin{aligned} \mathbf{a}&=(\tfrac{1}{2},\sqrt{3}/2,0)a\ , \\ \mathbf{b}&=(\tfrac{1}{2},-\sqrt{3}/2,0)a\ , \\ \mathbf{c}&=(0,0,c/a)a\ , \end{aligned} \tag{6}$$

where c/a is the axial ratio. There are four atoms per hexagonal unit cell. Their positions in units of **a**, **b**, and **c** are A at $(0,0,0)$ and $(\frac{2}{3},\frac{1}{3},\frac{1}{2})$ and B at $(0,0,u)$ and $(\frac{2}{3},\frac{1}{3},u+\frac{1}{2})$, where u denotes the dimensionless cell-internal structural parameter. Unlike the ZB case, there are now two distinct nearest-neighbor anion-cation bond lengths: one bond of equal lengths $R^{(1)}=uc$ and three bonds of equal lengths $R^{(2)}=a\sqrt{\frac{1}{3}+(\frac{1}{2}-u)^2(c/a)^2}$. For an ideal W structure, $c/a=\sqrt{\frac{8}{3}}$ and $u=\frac{3}{8}$, hence $R^{(1)}=R^{(2)}$. The independent structural parameters that need to be determined for the W structure are hence $\{V,c/a,u\}$, where V is the volume of the unit cell.

To find the equilibrium values of these structural parameters, we calculate the total energy at four lattice constant values, fitting $E(a)$ with Birch's equation of state[32] to get the equilibrium volume $V_{\rm eq}$ and $E(V_{\rm eq})$. For the W structure this minimization is carried out initially for $c/a=(c/a)_0=\sqrt{\frac{8}{3}}$ and $u=u_0=\frac{3}{8}$, finding $E[V_{\rm eq},(c/a)_0,u_0]$. We then calculated $E(V_{\rm eq},c/a,u_0)$ at three c/a values, finding the minimizing value $(c/a)_{\rm eq}$. Finally, we compute the quantum-mechanical forces at the configuration $[V_{\rm eq},(c/a)_{\rm eq},u]$ for two u values and displace all atoms to reduce the forces below 0.001 Ry/a.u. This establishes the final equilibrium geometry.

Detailed convergence tests were carried out to find the basis-set size and number of Brillouin-zone integration points needed to establish a maximum error in $\Delta E^{\rm LDF}_{\rm W-ZB}$ below 2 meV/atom. For the plane-wave pseudopotential method we find that this precision level required a

TABLE I. Calculated and measured structural parameters of ZB and W phases of some binary octet compounds. a and c are lattice constants (in Å) and u is the cell-internal structural parameter in the W structure. $\Delta E_{\rm W-ZB}$ is the relaxed W−ZB energy difference and $\delta E_{\rm rel}$ is the piece of $\Delta E_{\rm W-ZB}$ due to $c/a\neq\sqrt{\frac{8}{3}}$ and $u\neq\frac{3}{8}$ relaxation.

		Wurtzite				ZB		
		a (Å)	c (Å)	$\frac{c}{a}$	u	a (Å)	$\Delta E_{\rm W-ZB}$ (meV/atom)	$\delta E_{\rm rel}$ (meV/atom)
AlN	present	3.099	4.997	1.612	0.381	4.365	−18.41	−2.7
	Expt.[a]	3.112	4.9798	1.6004				
	Theor.[b]	3.129	4.988	1.594	0.3825			
InN	present	3.536	5.709	1.615	0.380	4.983	−11.44	−0.28
	Expt.[c]	3.5446	5.7034	1.6090				
	Expt.[d]					4.980		
GaN	present	3.095	5.000	1.633	0.378	4.364	−9.88	−0.32
	Expt.[e]	3.192	5.196	1.6278		4.531		
	Theor.[f]	3.126	5.119	1.6377	0.3767	4.419	∼−10.6	
	Theor.[g]	3.21					∼−15	
	Theor.[h]	3.043	4.969	1.6340	ideal		−9.52	
AlP	present	3.826	6.286	1.643	0.375	5.421	3.6	−0.05
	Expt.[i]					5.467		
AlAs	present	3.979	6.497	1.633	0.376	5.620	5.8	−0.15
	Expt.[j]					5.660		
GaP	present	3.759	6.174	1.643	0.374	5.328	9.18	−0.65
	Expt.[k]					5.4506		

TABLE I. (*Continued*).

		Wurtzite				ZB		
		a (Å)	c (Å)	$\frac{c}{a}$	u	a (Å)	ΔE_{W-ZB} (meV/atom)	δE_{rel} (meV/atom)
GaAs	present	3.912	6.441	1.647	0.374	5.654	12.02	−0.35
	Expt.[l]					5.65325		
C	present	2.490	4.144	1.665	0.374	3.539	25.3	−0.76
	Expt.[m]	2.51	4.12	1.6414				
	Expt.[n]					3.5670		
	Theor.[o]	2.50	4.14	1.656			30	
Si	present	3.800	6.269	1.650	0.374	5.392	11.72	−0.76
	Expt.[p]					5.43075		
	Theor.[q]						10	
CdS	present	4.121	6.682	1.621	0.377	5.811	−1.1	−0.4
	Expt.[r]	4.1367	6.7161	1.6235		5.818		
ZnS	present	3.777	6.188	1.638	0.375	5.345	3.1	−0.1
	Expt.[s]	3.8230	6.2605	1.6378				
	Expt.[t]					5.4102		
	Theor.[u]						1.865	
ZnSe	present	3.974	6.506	1.637	0.375	5.618	5.3	−0.5
	Expt.[v]	4.003	6.540	1.6338				
	Expt.[w]					5.6676		
ZnTe	present	4.273	6.989	1.636	0.375	6.045	6.4	−0.1
	Expt.[x]					6.009		

[a]Reference 34, at $T=298$ K.
[b]Reference 35, using plane-wave pseudopotentials with the Wigner exchange correlation, a cutoff basis set of 34 Ry, and 6 and 10 special **k** points for W and ZB.
[c]Reference 36.
[d]Reference 37.
[e]Reference 20, at room temperature.
[f]Reference 38, using plane-wave pseudopotentials with the Wigner exchange correlation, a cutoff basis set of 34 Ry, and 6 and 10 special **k** points for W and ZB.
[g]Reference 39, at $c/a=1.624$ and ideal u.
[h]Reference 40, using the plane-wave pseudopotentials method, and 30 and 60 special **k** points for W and ZB.
[i]Reference 41.
[j]Reference 42, at $T=291.15$ K.
[k]Reference 43, at room temperature.
[l]Reference 44, at $T=300$ K.
[m]Reference 45.
[n]Reference 46.
[o]Reference 47, using plane-wave pseudopotentials with Hedin-Lundquist exchange correlation, a cutoff basis set of 64 Ry, and 21 and 10 special **k** points for W and ZB, respectively.
[p]Reference 48, at $T=287.15$ K.
[q]Reference 49, using plane-wave pseudopotentials with Wigner exchange correlation, a cutoff basis set of 11.5 Ry, and 27 and 28 special **k** points for W and ZB, respectively.
[r]Reference 50, at room temperature.
[s]Reference 51, at room temperature.
[t]Reference 52, at $T=298$ K.
[u]Reference 53, using plane-wave pseudopotentials with Ceperley-Alder exchange-correlation, a cutoff basis set of 25 Ry, and 16 sampling **k** points per plane, in ideal W.
[v]Reference 14.
[w]Reference 54, at room temperature.
[x]Reference 55.

kinetic-energy basis-set cutoff value of 50 Ry for AlN, GaN, and InN, and 20 Ry for GaAs, AlAs, GaP, AlP, and Si. In the LAPW method this requires a kinetic-energy basis-set cutoff such that $K_{\max}R_{\min}^{\mathrm{MT}}=8.0$, where $K_{\max}$ is the square root of the kinetic energy and $R_{\min}^{\mathrm{MT}}$ is the muffin-tin radius. The spherical harmonic expansion inside the muffin-tin radius includes terms up to angular momentum $l=8$. The muffin-tin radii used in this study are $R=1.41$ a.u. for C; 2.29 and 2.00 a.u. for Zn and S in ZnS; 2.34 and 2.14 a.u. for Zn and Se in ZnSe; 2.40 and 2.40 a.u. for Zn and Te in ZnTe; and 2.56 and 2.12 a.u. for Cd and S in CdS. In conducting the structural optimizations we used for the Brillouin-zone integrations 10 and 14 special **k** points for the ZB and W structures, respectively. These special **k** points correspond to the (4,4,4) and (6,6,4) mesh points in the notation of Monkhorst and Pack.[33] We then increased the number of **k** points to converge $\Delta E_{AB}^{\mathrm{LDF}}$ at the final configuration to the accuracy of 2 meV/atom. For most of the compounds, this required a **k** mesh of (6,6,6) (28 special **k** points) for ZB and (8,8,4) (20 special **k** points) for W. In going to the denser **k**-points mesh, the largest change found in $\Delta E_{\mathrm{W-ZB}}^{\mathrm{LDF}}$ was 6 meV/atom for Si (which, therefore, required a larger set of 28 ZB and 20 W **k** points to reach ≤ 2 meV/atom error) but the average change was about 2 meV/atom or lower.

III. COMPARISON OF $\Delta E_{\mathrm{W-ZB}}^{\mathrm{LDF}}$ WITH EXPERIMENT AND PREVIOUS CALCULATIONS

Table I[14,20,34–55] compares the calculated equilibrium lattice constants, a_{eq}, the axial ratio c/a, and the energy difference $\Delta E_{\mathrm{W-ZB}}^{\mathrm{LDF}}$ with the experimental values (where available) and with the other theoretical calculations. Comparing the structural parameters with experiment, we find that the calculated equilibrium lattice constants are uniformly smaller than the experimental values by up to 2%. The calculated c/a ratios are within 0.4% of experiment. Interestingly, the calculated c/a ratios for the W-stable compounds (CdS, AlN, and InN) are smaller than the ideal value $(c/a)_0=\sqrt{\frac{8}{3}}$ [that of GaN is close to $(c/a)_0$], while the ZB-stable compounds (AlP, GaP, GaAs, ZnS, ZnSe, and ZnTe) have $c/a>(c/a)_0$, except for AlAs, which is slightly smaller than but very close to $(c/a)_0$. The diamond-stable crystals C and Si have significantly larger c/a ratios than all the ZB-stable compounds. This agrees with the phenomenological correlation established by Chelikowsky and Phillips.[25] In general, the calculated u values are very close to the ideal $u_0=\frac{3}{8}$ value, except for AlN, where the singlet bond length is slightly larger than the triplet bond length.

There are other theoretical calculations of $\Delta E_{\mathrm{W-ZB}}^{\mathrm{LDF}}(AB)$ for a number of compounds: GaN,[38–40] C,[47] and ZnS.[53] The results and methods of calculations are summarized in Table I. Our $\Delta E_{\mathrm{W-ZB}}^{\mathrm{LDF}}(\mathrm{ZnS})=3.1$ meV/atom value is within 1 meV/atom of the calculation of Engel and Needs,[53] and our $\Delta E_{\mathrm{W-ZB}}^{\mathrm{LDF}}(\mathrm{GaN})=-9.9$ meV/atom is within 0.7 meV/atom of the value of Van Camp, Van Doren, and Devreese[38] and within 0.3 meV/atom of the value of Min, Chan, and Ho.[40] Kunc *et al.* calculated $\Delta E_{\mathrm{W-ZB}}^{\mathrm{LDF}}(\mathrm{GaN})$ for the *experimental* c/a ratio and for the ideal $u=\frac{3}{8}$ value, finding -15 meV/atom. Our $\Delta E_{\mathrm{W-ZB}}^{\mathrm{LDF}}(C)$ is 5 meV/atom higher than the results of Fahy *et al.* The last column of Table I gives the relaxation correction $\delta E_{\mathrm{W-ZB}}^{\mathrm{LDF}}(AB)$ to the W–ZB energy difference, i.e., the energy difference between $\Delta E_{\mathrm{W-ZB}}^{\mathrm{LDF}}(AB)$ calculated for the relaxed W structure and $\Delta E_{\mathrm{W-ZB}}^{\mathrm{LDF}}(AB)$ in which the W structure is assumed to have the ideal c/a and u values. The relaxation energy $\delta E_{\mathrm{W-ZB}}^{\mathrm{LDF}}(AB)$ is generally smaller than 1 meV/atom, except for AlN, where it is -2.7 meV/atom.

IV. SCALING OF $\Delta E_{\mathrm{W-ZB}}(AB)$ WITH ATOMISTIC COORDINATES

Having established an internally consistent set of directly calculated W–ZB energy differences for a series of compounds, we now attempt to model this in terms of atomic properties.

The simplest possible scaling is between $\Delta E_{\mathrm{W-ZB}}^{\mathrm{LDF}}(AB)$ and the difference $\Delta\chi=|\chi(A)-\chi(B)|$ in global electronegativities[56] or the difference $\Delta r=|r_A-r_B|$ in tetrahedral atomic radii.[57] This is shown in Fig. 4. The overall quantity of the fit is good (rms errors of 4.0 and 5.2 meV/atom, respectively), indicating that large $\Delta\chi$ or large Δr favor the W structure. However, (i) these fits do not discriminate C from Si and Ge, whereas the calculated differences are big: $\Delta E_{\mathrm{W-ZB}}^{\mathrm{LDF}}$ is 25.3, 11.7, and 14 meV for C, Si, and Ge,[49] respectively. This failure suggests that we may need to search for an atomistic scale that incorporates some *orbital character,* since the *global* electronegativity or atomic sizes do not suffice to capture the trends in the homopolar ($A=B$) systems. Furthermore, (ii) there is room for improvement in the quality of the fit: we would like to reduce the rms error to 2–3 meV. To further search for scaling between $\Delta E_{\mathrm{W-ZB}}^{\mathrm{LDF}}$ and atomistic coordinates, we note that the tendency towards stabiliza-

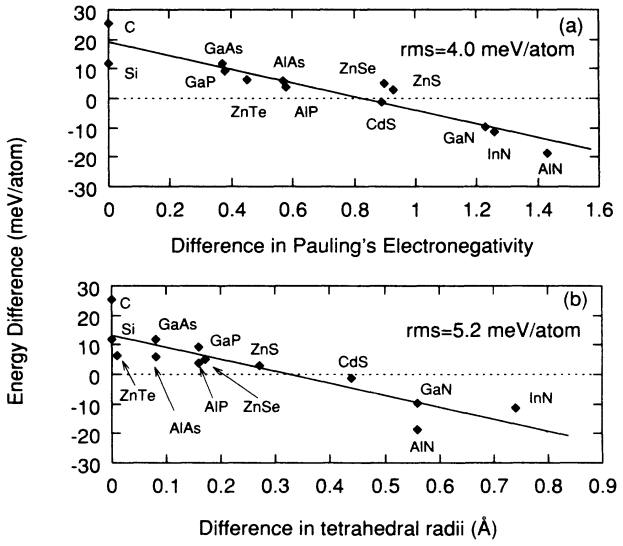

FIG. 4. The linear correction between the LDF-calculated W–ZB energy difference $\Delta E_{\mathrm{W-ZB}}^{\mathrm{LDF}}(AB)$ and (a) Pauling's electronegativity difference (Ref. 56), and (b) the difference in tetrahedral radii (Ref. 57) of A and B atoms.

TABLE II. r_s and r_p orbital radii (in Å) from the turning points of the screened nonrelativistic atomic pseudopotential [Zunger and Cohen (Refs. 23 and 24)], and from the maximum of the scalar-relativistic atomic orbitals $rR_{nl}(r)$.

	Pseudopotential orbital radii		Wave-function orbital radii	
	r_s	r_p	r_s	r_p
Be	0.64	0.44	2.041	2.282
B	0.48	0.315	1.519	1.561
C	0.39	0.25	1.216	1.191
N	0.33	0.21	1.017	0.966
O	0.285	0.18	0.874	0.813
F	0.25	0.155	0.767	0.703
Mg	0.90	1.13	2.515	3.496
Al	0.77	0.905	2.063	2.635
Si	0.68	0.74	1.774	2.145
P	0.60	0.64	1.566	1.827
S	0.54	0.56	1.407	1.598
Cl	0.50	0.51	1.279	1.424
Ca	1.32	1.68	3.327	4.370
Mn	0.99	1.23		
Cu	0.88	1.16	2.260	3.493
Zn	0.82	1.06	2.081	3.022
Ga	0.76	0.935	1.886	2.513
Ge	0.72	0.84	1.733	2.192
As	0.67	0.745	1.609	1.966
Se	0.615	0.67	1.504	1.784
Br	0.58	0.62	1.414	1.656
Ag	1.045	1.33	2.491	3.639
Cd	0.985	1.23	2.327	3.238
In	0.94	1.11	2.149	2.810
Sb	0.83	0.935	1.890	2.310
Te	0.79	0.88	1.788	2.143
I	0.755	0.83	1.699	2.007
Hg	1.07	1.34	2.209	3.157

tion of the W structure increases with the electronegativity difference $|\chi(A)-\chi(B)|$ [Fig. 4(a)] and that the *orbital* ionization energy and therefore, the *orbital* electronegativity $\chi_l(A)$ scales[24] as $1/r_l(A)$. This suggests a scaling [Eq. (3)] of $\Delta E_{W-ZB}(AB)$ with

$$\tilde{R}_\sigma(A,B)=\frac{R_\sigma(A,B)}{(r_p^A+r_s^A)(r_p^B+r_s^B)}$$

and (7)

$$\tilde{R}_\pi(A,B)=\frac{R_\pi(A,B)}{(r_p^A+r_s^A)(r_p^B+r_s^B)} .$$

To test this scaling we have used three sets of orbital radii r_l: (i) the density-functional pseudopotential radii of Zunger and Cohen,[23,24] (ii) the radii at which the all-electron atomic orbitals $rR_{nl}(r)$ have their outer maximum, and (iii) the nodal radii of Zhang, Cohen, and Phillips.[58] Table II lists the first two sets of radii for the pertinent elements.

Fitting the three parameters $\{E_0,\alpha,\lambda\}$ in the model energy of Eqs. (3) and (4),

$$\Delta E^M_{W-ZB}(AB)\equiv E_0+\alpha[\tilde{R}_\sigma(A,B)+\lambda\tilde{R}_\pi(A,B)] , \quad (8)$$

to the 13 calculated $\Delta E^{LDF}_{W-ZB}(AB)$ values yields a standard deviation of 2.8 meV/atom using the Zunger-Cohen pseudopotential radii. Correcting these radii for relativistic effects using the procedure of Ref. 58 reduces the standard deviation slightly (to 2.7 meV/atom). The standard deviation using the (relativistic) wave-function maximum radii or the nodal radii of Zhang, Cohen, and Phillips is 3.3 meV/atom. Figure 5 shows the correlation between the model energies ΔE^M_{W-ZB} of Eq. (8) and ΔE^{LDF}_{W-ZB} using two different sets of radii. In both cases the quality of the fit approaches the underlying precision with which ΔE^{LDF}_{W-ZB} can presently be computed.

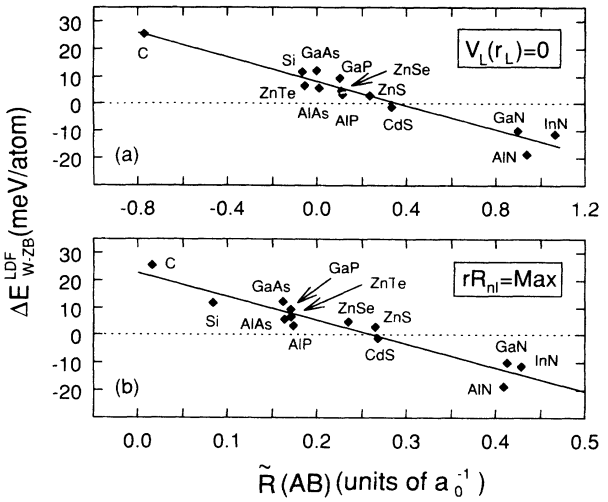

FIG. 5. The linear correction between the LDF-calculated W−ZB energy difference $\Delta E^{LDF}_{W-ZB}(AB)$ and the orbital coordinate $\tilde{R}(A,B)$ of Eq. (3), calculated from (a) the orbital radii given in Ref. 24. The parameters of the fit [Eqs. (3) and (4)] are $E_0=8.137$ meV, $\alpha=-22.152$, and $\lambda=-1.13$. (b) The wave-function orbital radii coordinate. The parameters of the fit are $E_0=22.67$, meV, $\alpha=-85.74$, and $\lambda=1.742$.

The choice of $\tilde{R}_\sigma,\tilde{R}_\pi$ as of the scaling coordinates in Eq. (8) appears to give the best fit with a maximum of three parameters. We noted the following: (i) Although the structural separation maps (Fig. 3) indicate that R_σ is the crucial coordinate in affecting a ZB−W separation, a quantitative fit shows that use of R_σ alone raises the rms error of a linear fit to 5.28 meV/atom. Indeed, omitting the orbital dependence of the coordinates [i.e., setting $r_s=r_p$, hence $R_\pi(AB)=0$] fails to distinguish between C, Si, and Ge as $R_\sigma(C)=R_\sigma(Si)=R_\sigma(Ge)=0$. In fact (Fig. 2), $\Delta E^{LDF}_{W-ZB}(C)\gg\Delta E^{LDF}_{W-ZB}(Si)$. Therefore, we need to include R_π in our model. (ii) The improvement in the fit in going from R_σ to $\tilde{R}_\sigma$ can be significant: the rms error is reduced by 8% for the pseudopotential orbital radii, and by 21% using the wave-function orbital radii. (iii) There is a further improvement in going from $\tilde{R}_\sigma$ to $\tilde{R}_\sigma+\lambda\tilde{R}_\pi$: by 42% using the pseudopotential orbital radii, and by 14% using the wave-function orbital radii. (iv) We note that the use of Phillips' $C-E_h$ scale produces almost a double rms error of 5.4 meV/atom. We will next use our model energy difference of Eqs. (7) and (8) to predict chemical trends in the W−ZB stability.

V. CHEMICAL TRENDS IN $\Delta E_{W-ZB}(AB)$

A. Global trends

Figure 6 shows the predicted ΔE^M_{W-ZB} in the anion series of (a) III-V, (b) II-VI, (c) I-VI, and (d) IV-IV compounds using Eqs. (7) and (8) and the pseudopotential orbital radii. Figure 7 shows analogous results using the wave-function orbital radii. We find that the stability of these phases is generally delineated by a single coordinate, i.e., $\tilde{R}(A,B)$ of Eq. (3). When $\tilde{R}$ from the pseudopotential orbital radii is between $\tilde{R}_c^{(1)}=0.38(a_0^{-1})$ [where $\Delta E^M(\tilde{R}_c^{(1)})=0$] and $\tilde{R}_c^{(2)}=-0.20(a_0^{-1})$, the ZB structure is stabler, whereas for $\tilde{R}$ between $\tilde{R}_c^{(1)}$ and $\tilde{R}_c^{(3)}=1.2(a_0^{-1})$ the W structure is stabler. Excluding for the moment those compounds for which $|\Delta E^M_{W-ZB}|$ is comparable to the standard deviation σ of the fit, we find that our model correctly describes, with only a few exceptions (see below), the overall W vs ZB structure preferences established experimentally:[1–5] column III nitrides and column IIB oxides tend to adopt the W structure, whereas heavier anions stabilize the ZB structure. The apparent errors in the predictions relative to the previously accepted structural designations are as follows.

(i) Using the pseudopotential orbital radii, we find that CdSe, HgSe, and MgTe believed[3–5,21–25] to have the W ground state at low temperature are predicted here to be stabler in the ZB structure. A recent careful examination

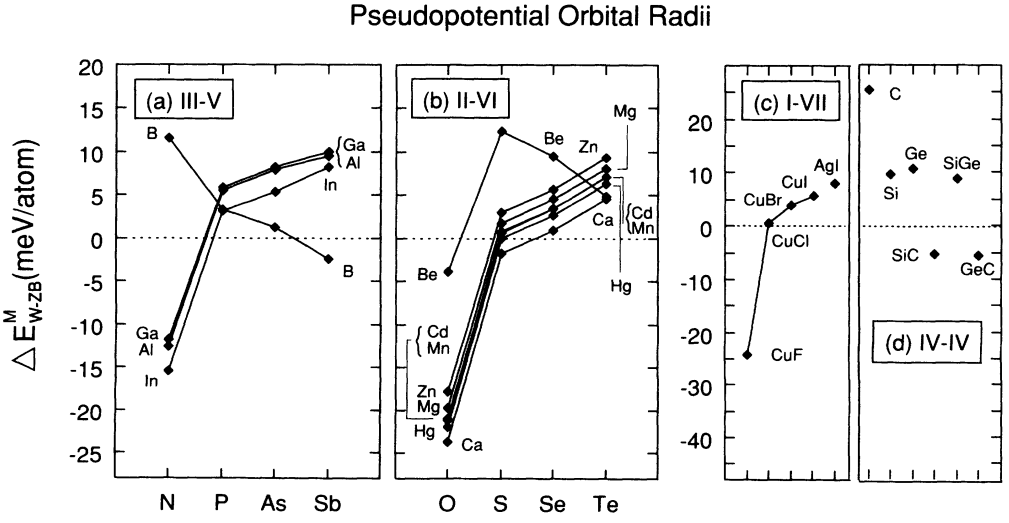

FIG. 6. Predicted W−ZB energy differences $\Delta E^M_{W-ZB}(AB)$ [Eq. (3)] for (a) the III-V series, (b) the II-VI series, and (c) the I-VII and IV-IV series from the classical orbital radii (Refs. 23 and 24).

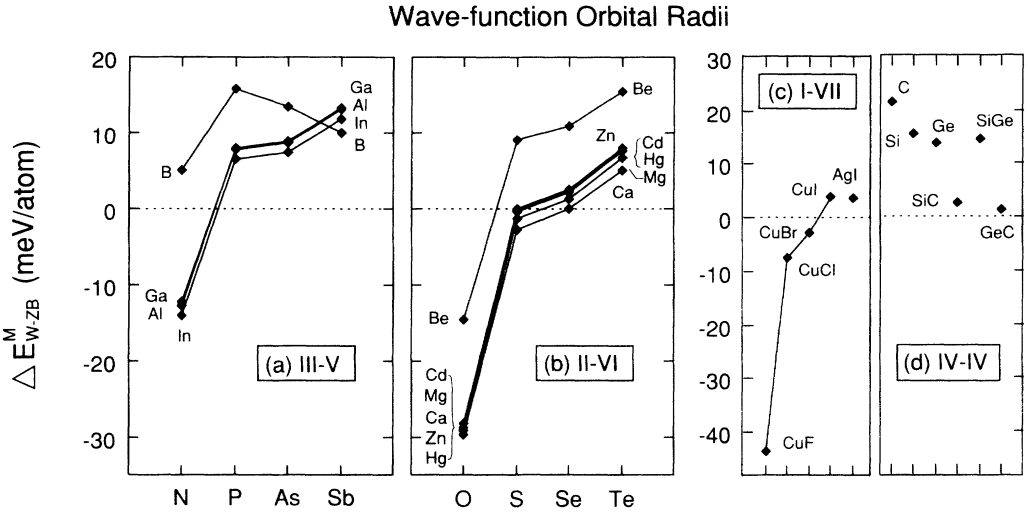

FIG. 7. Predicted W−ZB energy differences $\Delta E^{M}_{W-ZB}(AB)$ from the wave-function orbital radii [Eq. (8)] for (a) the III-V series, (b) the II-VI series, and (c) the I-VII and IV-IV anion series.

of the ZB→W phase transition in CdSe (Ref. 10) established conclusively, however, that ZB is the stable low-temperature phase, in agreement with our result. Similarly, HgSe was previously erroneously designated to have the W ground state;[3,5,23,24] it is ZB at low temperatures.[1] To examine these cases more closely, we have calculated ΔE^{LDA}_{W-ZB} of CdSe and HgSe using the LAPW method. Table III gives the calculated structural parameters. We find ΔE^{LDA}_{W-ZB} of 1.4 and 6.9 meV/atom, respectively, hence the ZB structure is indeed stabler, as suggested by experiment.[1,10] The quantitative agreement with the model is mediocre: the model predicts 3.3 and 2.7 meV/atom, respectively. (ii) Using the wave-function-maximum orbital radii, ZnS, CuCl, and CuBr

TABLE III. Lattice parameters in (Å) of MgTe, BeTe, and BeS, calculated by the plane-wave nonlocal pseudopotential method (Ref. 24) and of CdSe and HgSe, calculated using the LAPW method. The results are compared with experimental data (in parentheses). The W−ZB energy difference of these five systems was not included in the fit to the model. The last two columns compare the energy difference (meV/atom) for the LDF from Eq. (2) and for the model prediction from Eq. (4).

		a	$\frac{c}{a}$	c	u	ΔE^{LDF}_{W-ZB}	ΔE^{M}_{W-ZB}
	ZB	6.364					
	W	4.505(4.52)[a]	1.633(1.6327)[a]	7.358(7.38)[a]	0.376		
MgTe						−1.0	8.0
	NaCl	5.846					
	NiAs	4.142	1.624	6.724	0.0		
	ZB	5.537(5.6269)[b]					
BeTe						8.8	12.4
	W	3.346	1.640	5.485	0.374		
	ZB	4.739(4.8630)[b]					
BeS						6.0	4.9
	W	3.338	1.651	5.510	0.374		
	ZB	6.045					
CdSe						1.4	3.3
	W	4.274	1.636	6.991	0.375		
	ZB	6.099					
HgSe						6.9	2.7
	W	4.310	1.639	7.064	0.375		

[a]Reference 60.
[b]Reference 61, at room temperature.

are predicted to be W instead of ZB. (iii) Using Phillips' coordinates,[21] E_h and C in the fit of Eqs. (3) and (4) leads also to a twofold increase in the standard deviation of the fit and predicts incorrectly ZnS, ZnSe, CuCl, CuBr, and CuI to be W. Hence, despite the fact that (E_h, C) provide a good diagrammatic separation of different crystal structures, they do not exhibit a quantitative scaling with the *energy difference* $\Delta E_{\alpha\beta}(AB)$ as well as the $(\tilde{R}_\sigma, R_\pi)$ from the orbital radii coordinates do.

Considering next compounds for which $|\Delta E^M_{W-ZB}|$ is small (≤ 3 meV), we identify materials that exhibit strong W-ZB polytypism: CdS, CuCl, and ZnS with ΔE^M values of 0.7, 0.6, and 2.9 meV, respectively.

B. The case of MgTe

The only significant discrepancy between our model using the pseudopotential orbital radii and the current experimental data concerns MgTe: Both Figs. 6 and 7 predict MgTe to be stabler in the ZB structure, while, experimentally, MgTe appears in the W structure.[59] This result was obtained by Zachariasen,[59] who grew MgTe powder, finding hexagonal reflection patterns in this highly hygroscopic nonstoichiometric mixture of Mg+MgO +MgTe. However, it is not obvious from these experiments whether W is the stable low-temperature phase (in which case our prediction is incorrect) or W is stable only at high temperature (in which case our result does not necessarily conflict with experiments).[59]

To resolve this question we have calculated the LDF total energy of MgTe in the ZB, W, NaCl, and NiAs structures. The structural parameters are summarized in Table III.[60,61] We find that the energy differences relative to the ZB phase are 0, −1.0, −1.3, and −15 meV/atom, respectively. Hence, both *the W and ZB forms of MgTe are predicted to be unstable at low temperatures relative to the NiAs-type structure.* The situation here is analogous to what was found[62] in Mn chalcogenides, where MnO, MnS, and MnSe have the NaCl structure, but MnTe has the NiAs structure. Furthermore, the metastable ZB form of MnTe can be stabilized during growth.[62] We hence suspect that the experimental observations[59] of W as the structure of MgTe pertains to the *high-temperature* stable phase. The stablest *low-temperature* phase is predicted by the LDF to be NiAs. This prediction awaits experimental testing. Note, however, that the LDF predicts ZB to be slightly more stable than W, in conflict with the model.

C. Trends with anions

With the exception of first-row cation compounds, we find that ΔE^M_{W-ZB} increases monotonically for all III-V, II-IV, and I-VII compounds as the anion becomes heavier (i.e., progressing down a column in the Periodic Table). Compounds with first-row cations show mostly the reverse trends. These trends can be understood in terms of the atomic sizes (which are proportional to $r_s + r_p$). For most elements the cations are larger than the anions. As we go down a row of anions the anion size increases, which in turn causes the size difference $|r_A - r_B|$ to decrease favoring the zinc-blende polytype for the heavier elements. The exception to this rule is the first-row cations whose sizes are comparable to the anions. Indeed, for the pseudopotential radii, the sizes of the first-row cations are smaller than the size of the largest anions causing a minimum in $|r_A - r_B|$ with a corresponding maximum in the wurtzite–zinc-blende energy difference in the middle of the anion column. This reflects that the anion dependence of ΔE^M is generally monotonic with respect to the anion position in a column, except for the compounds with cations in the first row. This also explains the possibility for chemical trends in boron pnictides and beryllium chalcogenides that are not monotonic.

The prediction from the orbital radii and the wave-function maximum are significantly different for compounds containing a first-row element, e.g., the boron pnictides and the beryllium chalcogenides. While the pseudopotential orbital radii predict

$$\Delta E^M_{W-ZB}(\text{BeS}) > \Delta E^M_{W-ZB}(\text{BeSe}) > \Delta E^M_{W-ZB}(\text{BeTe}) \quad (9)$$

[Fig. 6(b)], the wave-function maximum orbital radii predict

$$\Delta E^M_{W-ZB}(\text{BeS}) < \Delta E^M_{W-ZB}(\text{BeSe}) < \Delta E^M_{W-ZB}(\text{BeTe}) \quad (10)$$

[Fig. 7(b)]. To check which trend is correct, and at the same time examine the predictive ability of our model of Eqs. (7) and (8), we have calculated the W−ZB energy difference ΔE^{LDF}_{W-ZB} in BeS and BeTe using the pseudopotential LDF method. We find (see Table III for calculated lattice parameters)

$$\Delta E^{LDF}_{W-ZB}(\text{BeS}) = 8.8 \text{ meV/atom}$$

and (11)

$$\Delta E^{LDF}_{W-ZB}(\text{BeTe}) = 6.0 \text{ meV/atom}$$

clearly favoring the pseudopotential orbital radii of Eq. (9). Hence, the trend shown by the pseudopotential orbital radii [Eq. (9) and Fig. 6(b)] is correct. Table III summarizes the quantitative predictive ability of the model for five compounds not used in the fit. The difference is about 4 meV/atom for all except MgTe. We have no explanation for this unexpected error.

Using these radii, we can now formulate from Fig. 6 the anion rule of W−ZB stability: The ZB structure is monotonically stabilized over the W structure as the anion becomes heavier in all except first-row cation compounds. In the latter case, heavy anions tend to stabilize the W structure.

D. Trends with cations

Figures 8 and 9 show the trend of ΔE^M_{W-ZB} with respect to the cation position in a Periodic Table column. Comparison with Figs. 6 and 7 show that the choice of cation if far less decisive in establishing ZB vs W preferences than the choice of anions. Again, the exception are compounds with first-row anions. We see that oxides have much lower ΔE^M_{W-ZB} values than sulphides,

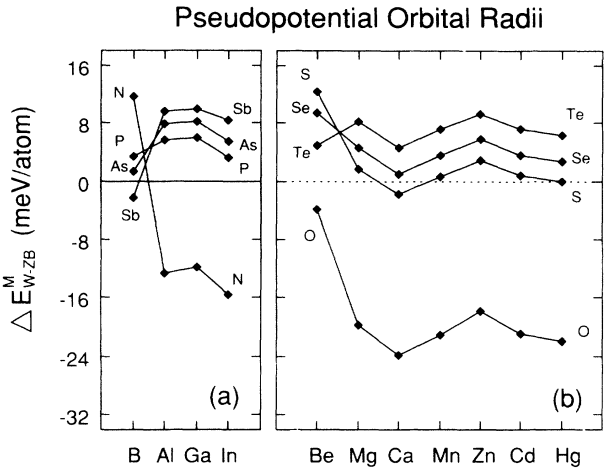

FIG. 8. Anion trends from the pseudopotential orbital radii (Refs. 23 and 24).

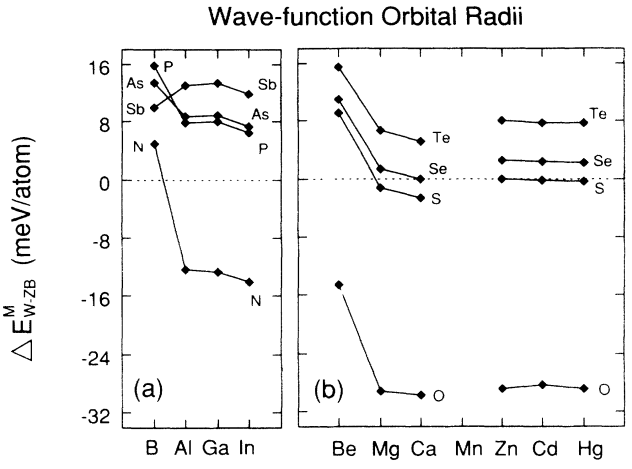

FIG. 9. Anion trends from the wave-function orbital radii.

selenides, and tellurides. Like oxides, nitrides also strongly stabilize the W structure over ZB.

It is interesting to note the trend for the III-V compounds. We find

$$\Delta E^{M}_{W-ZB}(\mathrm{In}X) < \Delta E^{M}_{W-ZB}(\mathrm{Al}X) < \Delta E^{M}_{W-ZB}(\mathrm{Ga}X) \quad (12)$$

for X=P,As,Sb using either choice of orbital radii [Figs. 8(a) and 9(a)]. This trend, unlike the anion trends of Figs. 6 and 7, is *nonmonotonic* with respect to the position of the column III cation in a Periodic Table row. Insofar as $\Delta E^{M}(A,B) \propto \tilde{R}(A,B)$ constitutes an orbital ionicity scale, this suggests AlX to be *more* ionic than GaX, in agreement with the calculation of Christensen, Satpathy, and Pawlowska,[63] but in conflict with Phillips' scale.[21]

E. ΔE_{W-ZB} for compounds that are unstable in the W or ZB structures

From the prediction of pseudopotential orbital radii, we find that compounds whose ground state is the NaCl structure are divided into two groups in terms of the order of their metastable phases: MgO, CaO, MnO, and CdO are predicted to favor metastable W structure (with ΔE^{M}_{W-ZB} of -19.7, -23.8, -21.2, and -21.0 meV/atom, respectively), while CaTe and MgSe are predicted to favor a metastable ZB structure (with ΔE^{M}_{W-ZB} of $+4.5$ meV/atom for both). For C (stable in the graphite form), we find that the metastable cubic (diamond) structure is considerably lower in energy than the W form ($\Delta E^{M}_{W-ZB}=25$ meV/atom). Both SiC and GeC are found on the W side of the W/ZB border (the actual ground state of SiC is apparently the hexagonal 6H polytype,[4] while SiGe is predicted to be strongly ZB.

VI. SUMMARY

Angular-momentum-dependent pseudopotential orbital radii, wave-function radii, and dielectric models, all achieve good diagrammatic structural separation between the wurtzite and zinc-blende polytypes for octet semiconductors. We find that these coordinates also exhibit a linear correlation with the calculated LDA zinc-blende–wurtzite energy differences. The best fit is obtained for a scaled version of the first-principles pseudopotential orbital radii[23,24] where we obtain a standard deviation of 2.8 meV in the fit to a set of 13 calculated compounds whose W$-$ZB energy differences span $\sim$50 meV. Using this linear model we have studied trends in the set of all tetrahedrally coordinated octet compounds. We find that in general the zinc-blende phase is favored as the atomic number of the anion increases (anion rule). The exception to this rule is compounds containing first-row cations.

From the model predictions we propose that the previously accepted low-temperature ground-state structures of CdSe, HgSe, and MgTe should be revised. In particular, we find that MgTe should be stable in the NiAs structure. This awaits experimental verification.

ACKNOWLEDGMENT

This work was supported by the Office of Energy Research (OER) [Division of Materials Science of the Office of Basic Energy Science (BES)], U.S. Department of Energy, under Contract No. DE-AC-02-77-CH00178.

[1]P. Villars and L. Calvert, *Pearson's Handbook of Crystallographic Data for Intermetallic Phases* (American Society for Metals, Metals Park, OH, 1985).

[2]R. W. G. Wyckoff, *Crystal Structure*, 2nd ed. (Interscience, New York, 1963), Vol. 1.

[3]K. Schubert, *Kristallstruktren Zweikomponentiger Phasen* (Springer-Verlag, Berlin, 1964).

[4]*Structural Data of the Elements and Intermetallic Phases*, edited by K. H. Hellwege and A. H. Hellwege, Landolt-Börnstein, New Series, Group III, Vol. 6 (Springer-Verlag, Berlin, 1971); *ibid.* Vols. 17a and 17b; *ibid.* Vols. 17c and 17d.

[5]E. Parthe, *Crystal Chemistry of Tetrahedral Structures* (Gordon and Breach, New York, 1964).

[6]L. Patrick, D. R. Hamilton, and W. J. Choyke, Phys. Rev. **143**,

526 (1966).
[7]R. G. Humphreys, D. Bimberg, and W. J. Choyke, J. Phys. Soc. Jpn. **49** Suppl. A, 519 (1980).
[8]*Diamond, Silicon Carbide and Related Wide Bandgap Semiconductors,* edited by J. T. Glass, R. Messier, and N. Fujimori, MRS Symposia Proceedings No. 162 (Materials Research Society, Pittsburgh, 1990); Phys. Status. Solidi A **126**, K5 (1991).
[9]R. Rapoport and C. W. F. T. Pistorius, Phys. Rev. **172**, 838 (1968).
[10]V. A. Fedorov, V. A. Ganshin, and Yu. N. Korkishko, Phys. Status Solidi (A) **126**, K5 (1991).
[11]Y. M. Rumyantsev, F. A. Kuznetsov and S. A. Stroitelve, Kristallografiya **10**, 263 (1965) [Sov. Phys. Crystallogr. **10**, 212 (1965)].
[12]N. Samarth, H. Luo, J. K. Furdyna, S. B. Qadri, Y. R. Lee, A. K. Ramdas, and N. Otsuka, App. Phys. Lett. **54**, 2680 (1989).
[13]H. Luo, N. Samarth, F. C. Zhang, A. Pareek, M. Dobrowolska, J. K. Furdyna, K. Mahalingam, N. Otsuka, W. C. Chou, A. Petrou, and S. B. Qadri, Appl. Phys. Lett. **54**, 1783 (1991).
[14]W. M. Yim and E. J. Stofko, J. Electrochem. Soc. Solid-State Science Technol. **119**, 381 (1972).
[15]S. Froyen, S.-H. Wei, and A. Zunger, Phys. Rev. B **38**, 10 124 (1988).
[16]L. G. Schulz, J. Chem. Phys. **18**, 996 (1950).
[17]G. Berthold, Z. Phys. **181**, 333 (1964).
[18]H. Mittendorf, Z. Phys. **183**, 113 (1965).
[19]S. Minomura, O. Shimomura, K. Asaumi, H. Oyanagi, and K. Takemura, in *Proceedings of the Seventh International Conference on Amorphous and Liquid Semiconductor,* edited by W. E. Spear (Center for Industrial Consultancy and Liaison, University of Edinburgh, Edinburgh, Scotland, 1977), p. 53.
[20]R. C. Powell, G. A. Tomasch, Y.-W. Kim, J. A. Thornton, and J. E. Greene, in *Diamond, Silicon Carbide and Related Wide Band Gap Semiconductors,* edited by J. T. Glass, R. Messier, and N. Fujimori, MRS Symposia Proceedings No. 162 (Materials Research Society, Pittsburgh, 1990), p. 525.
[21]J. C. Phillips, *Bonds and Bands in Semiconductors* (Academic, New York, 1973).
[22]J. St. John and A. N. Bloch, Phys. Rev. Lett. **33**, 1095 (1974).
[23]A. Zunger and M. L. Cohen, Phys. Rev. Lett. **41**, 53 (1978).
[24]A. Zunger, Phys. Rev. B **22**, 5839 (1980); Phys. Rev. Lett. **44**, 582 (1980); in *Structure and Bonding in Crystal,* edited by M. O'Keeffe and A. Navrotsky (Academic, New York, 1981), Vol. 1, p. 73.
[25]J. R. Cheliowsky and J. C. Phillips, Phys. Rev. B **17**, 2453 (1978).
[26]P. Villars, J. Less Common Met. **92**, 215 (1983); **99**, 33 (1984); **102**, 199 (1984); P. Villars and F. Hulliger, *ibid.* **132**, 289 (1987).
[27]P. Villars, J. C. Phillips, and H. S. Chen, Phys. Rev. Lett. **57**, 3085 (1986); P. Villars and J. C. Phillips, Phys. Rev. B **37**, 2345 (1988); K. M. Rabe, A. R. Kortan, J. C. Phillips, and P. Villars, *ibid.* **43**, 6280 (1991).
[28]J. Ihm, A. Zunger, and M. L. Cohen, J. Phys. C **12**, 4409 (1979).
[29]S.-H. Wei and H. Krakauer, Phys. Rev. Lett. **55**, 1200 (1985), and references therein.
[30]Chin-Yu Yeh, Z. W. Lu, S. Froyen, and Alex Zunger, Phys. Rev. B **45**, 12 130 (1992).
[31](a) D. M. Ceperley and B. J. Alder, Phys. Rev. Lett. **45**, 566, (1980); (b) J. P. Perdw and A. Zunger, Phys. Rev. B **23**, 5048 (1981); (c) G. P. Kerber, J. Phys. C **13**, L189 (1980); (d) S. G. Louie, S. Froyen, and M. L. Cohen, Phys. Rev. B **26**, 1738 (1982).
[32]F. Birch, J. Geophys. Res. **83**, 1257 (1978).
[33]H. J. Monkhorst and J. K. Pack, Phys. Rev. B **13**, 5188 (1976).
[34]W. M. Yim and R. J. Paff, J. Appl. Phys. **45**, 1456 (1974).
[35]P. E. Van Camp, V. E. Van Doren, and J. T. Devreese, Phys. Rev. B **44**, 9056 (1991).
[36]V. A. Tyagai, A. M. Evstigneev, A. N. Krasiko, A. F. Malakhov, and V. Ya, Fiz. Tekh. Poluprovodn. **11**, 2142 (1977) [Sov. Phys. Semicond. **11**, 1257 (1977)].
[37]S. Strite, J. Ruan, D. J. Smith, J. Sariel, N. Manning, H. Chen, W. J. Choyke, and H. Morkoc, Bull. Am. Phys. Soc. **37**, 346, 1992.
[38]P. E. Van Camp, V. E. Van Doren, and J. T. Devreese, Solid State Commun. **81**, 23 (1992).
[39]A. Munoz and K. Kunc, Phys. Rev. B **44**, 10 372 (1991).
[40]B. J. Min, C. T. Chan, and K. M. Ho, Phys. Rev. B **45**, 1159 (1992).
[41]C. C. Wang, M. Zaheeruddin, and L. H. Spinar, J. Inorg. Nucl. Chem. **25**, 326 (1961).
[42]W. B. Pearson, *A Handbook of Lattice Spacings and Structure of Metals and Alloys* (Pergamon, Oxford, 1967).
[43]S. Kishino, Adv. X-Ray Anal. **16**, 367 (1973).
[44]C. M. H. Driscoll, A. F. W. Willoughby, J. B. Mullin, and B. W. Straughan, in *Gallium Arsenide and Related Compounds,* edited by J. Bok, IOP Conf. Proc. No. 24 (Institute of Physics and Physical Society, London, 1974), p. 275.
[45]F. P. Bundy, J. S. Kasper, J. Chem. Phys. **46**, 3437 (1967).
[46]J. Donahue, *The Structure of the Elements* (Krieger, Malabar, FL, 1982).
[47]S. Fahy and Steven G. Louie, Phys. Rev. B **36**, 3373 (1987).
[48]F. Godwod, R. Kowalcyzk, and Z. Szmid, Phys. Status Solidi A **21**, 227 (1974).
[49]K. J. Chang and M. L. Cohen, Phys. Rev. B **31**, 7819 (1985).
[50]W. R. Cook, Jr., J. Am. Ceram. Soc. **51**, 518 (1968).
[51]R. R. Reeber and G. W. Powell, J. Appl. Phys. **38**, 1531 (1967).
[52]J. C. Jamieson and H. H. Demarest, J. Phys. Chem. Solids **41**, 963 (1980).
[53]G. E. Engel and R. J. Needs, J. Phys. Condens. Matter **2**, 367 (1990).
[54]H. P. Singh and B. Dayal, Phys. Status. Solidi **23**, K93 (1967).
[55]T. Yao, in *The Technology and Physics of Molecular Beam Epitaxy,* edited by E. H. C. Parker (Plenum, New York, 1985), p. 313.
[56]L. Pauling, *The Nature of the Chemical Bond,* 3rd ed. (Cornell University Press, New York, 1960), pp. 90ff.
[57]W. B. Pearson, *Crystal Chemistry and Physics of Metals and Alloys* (Wiley, Toronto, 1972), p. 147.
[58]S. B. Zhang, M. L. Cohen, and J. C. Phillips, Phys. Rev. B **36**, 5861 (1987).
[59]W. Zachariasen, Z. Phys. Chem. **128**, 417 (1927).
[60]W. Klemm and K. Wahl, Anorg. Allg. Chem. **266**, 289 (1951).
[61]W. M. Yim, J. P. Dismukes, E. J. Stofko, and R. J. Paff, J. Phys. Chem. Solids **33**, 501 (1972).
[62]S.-H. Wei and A. Zunger, Phys. Rev. Lett. **56**, 2391 (1986), and references therein.
[63]N. E. Christensen, S. Satpathy, and Z. Pawlowska, Phys. Rev. B **36**, 1032 (1987).